Hindawi
Mathematical Problems in Engineering
Volume 2019, Article ID 7248072, 17 pages
https://doi.org/10.1155/2019/7248072

Research Article

A Protection Method Based on Feature Cosine and Differential Scheme for Microgrid

Lai Lei[1,2] **Cong Wang**[1] **Jie Gao**[3] **Jinjin Zhao**[2] **and Xiaowei Wang**[4,5]

[1] *China University of Mining & Technology, Beijing 100083, China*
[2] *Zhengzhou Electric Power College, Zhengzhou 450000, China*
[3] *Shanghai University of Electric Power, Shanghai 200090, China*
[4] *Xi'an Jiaotong University, Xi'an 710049, China*
[5] *Henan Polytechnic University, Jiaozuo 454000, China*

Correspondence should be addressed to Lai Lei; 1215894189@qq.com

Received 26 October 2018; Revised 25 January 2019; Accepted 19 February 2019; Published 10 March 2019

Academic Editor: Yakov Strelniker

The fault current level of microgrid is different between islanded mode and grid connected mode. This situation degrades the performance of traditional overcurrent protection schemes. Hence, this paper proposes a protection method based on feature cosine and differential scheme. Firstly, feature cosine is proposed; it employs ellipse equation and minimum least squares to quantify the united behavior about voltage and current. Secondly, fault current direction and feature cosine are analyzed when fault occurs at different locations of a typical microgrid, and then the difference of feature cosine between faulty and healthy section locations is obtained. Thirdly, based on feature cosine and differential scheme, the differential direction is defined and utilized to detect faulty section location. Lastly, various time domain simulation case studies, including different microgrid operation modes, grounding resistances, faulty types, faulty section locations, and noise influence, are conducted and demonstrate that the proposed protection has high accuracy.

1. Introduction

Due to climate concern, technological advancements, and government incentives, microgrids are emerging as a low-medium voltage energy network which include various types of distributed generation (DG) such as solar, wind, and geothermal [1, 2]. Some advantages of the presence of microgrids include reduction of power delivery loss, reduced greenhouse gases, and enhancement of power reliability.

However, the emergence of microgrids involves a lot of technical challenges, e.g., voltage and frequency control, stability problems, power quality, and so on, because microgrid operation, control, and protection are typically different from those of traditional power networks [3–5]. One of the major issues in microgrid is the microgrid protection. Different reasons responsible for this are as follows: (i) power flow may become bidirectional when DGs are integrated into the microgrid; (ii) fault current levels may be limited to 2~3 times the inverter-rated current; (iii) the microgrid may connect or disconnect DGs; (iv) the microgrid has two operation modes including islanded and grid connected modes; (v) zero and negative sequence currents cannot be neglected in normal conditions since single- and three-phase unbalanced loads are embedded into microgrids.

At present, scholars have proposed various methods to protect microgrids. Reference [6] proposes a three-stage approach to microgrid protection including offline analyses, online calculation, and real-time protection, which is based on establishing dynamic security model in microgrid. Reference [7] employs hysteresis control and maximum current RMS control to limit the fault current; it can make fault current have a percentage of fifth harmonic which is utilized to build protection strategy, but this method is only suitable for islanded microgrid. Reference [8] investigates protection issues related to LV microgrids and elaborates LV microgrid protection concepts comprehensively. Voltage and frequency relays are used as a point of common coupling relay, and directional overcurrent (DOC) relay is utilized for feeder

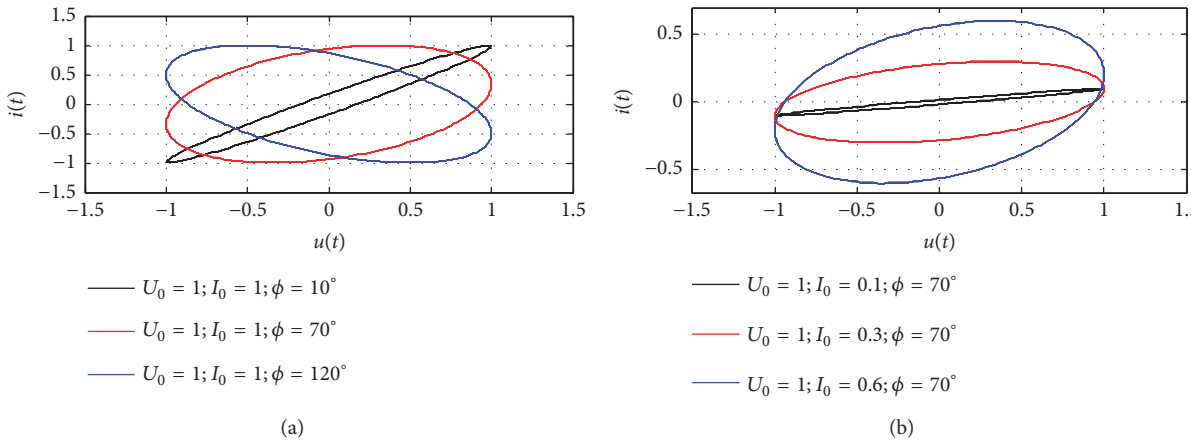

Figure 1: Elliptical behavior of a phase in a bus for different situations. (a) Elliptical behavior of a phase in a bus for different values of ϕ and (b) elliptical behavior of a phase in a bus for different values of I_0.

protection. DOC takes a long time to operate. Besides, with its operation, all of the feeder elements should be tripped. In [9, 10], sequence components, e.g., positive and negative sequence components, are employed to design the protection, but it can make relay coordination become more complex because of multiple settings. Reference [11] has proposed a novel fault location method based on the maximum oscillation magnitude of the transient voltage signal, but this method does not consider the three-phase microgrid. The d-q wavelet packet transform-based digital protection has been implemented to investigate several transient disturbances occurring in different parts of the microgrid system [12]; it suffers a problem about choosing suitable wavelet basis functions. Two time-frequency-based differential schemes, which can avoid the selection of wavelet basis functions, are presented for microgrid protection; one is the Hilbert-Huang transform [13], and the other is the generalized S-transform [14]. In these two works, how to find effective threshold is necessary. This problem can be avoided by some statistical classifiers; for instance, [15, 16] have used the three-phase voltage amplitude, voltage total harmonic distortions, and other 19 electrical features to build classifiers including Decision Tree and Naive Bayes, to detect fault and achieve protection; [17] has utilized combined wavelet transform and decision tree to detect and classify the fault; however, the protection strategies in [15, 16] are only designed for islanded microgrid, and the unbalanced loads situation is not considered in [17]. Reference [18] presents a data-mining-based intelligent differential protection scheme for the microgrid, but it uses 7 feature components, for example, the differential rate-of-change of frequency, the differential reactive power change with time and so on, but the shortcoming of this method is that it has much data needed to solve including many feature components and high sampling rates. This problem can also be found in [15–17].

Thus, compared with other differential methods, the contributions of this paper are as follows:

(1) This paper extracts the fault feature through solving the parameters of ellipse equation based on the current and voltage fault component. It can only use 5 sampling points to determine the parameters of ellipse which are employed to acquire polarity relationship between the busbar voltage and current.

(2) As for detection criteria, this paper uses ±1 to define the feature direction of busbar. It can decrease the difficulty of communication and avoid threshold selection for different operation modes of microgrid.

The rest of this paper is organized as follows. Section 2 employs ellipse equation and minimum least squares to acquire feature cosine to describe the united behavior about voltage and current. The microgrid structure and the reason why the feature cosine can be used are shown in Section 3. Section 4 discusses the change of feature cosine when fault occurs at different locations. Section 5 presents how to use the feature cosine to obtain the differential feature direction to detect faulty section location. Section 6 shows the performance of proposed method including different microgrid operation modes, grounding resistances, and faulty section locations. Moreover, the condition of unbalanced loads is taken into consideration.

2. Feature Cosine of One Phase in a Bus

2.1. Mathematical Background. The voltage and current signals in one phase of a bus at time t can be written as

$$u(t) = U_0 \sin(\omega t) \tag{1}$$

$$i(t) = I_0 \sin(\omega t - \phi) \tag{2}$$

where the angle ϕ is the delay between $i(t)$ and $u(t)$. U_0 and I_0 are the peak values of $u(t)$ and $i(t)$, respectively. ω is the angular velocity, $\omega=2\pi f$. In China system, $f=50$ Hz. $\cos(\phi)$ is defined as the feature cosine.

As for a bus, Figure 1 shows the united behavior of the voltage and current sine signals for one phase at different conditions. This behavior can be modeled using a conic section mathematical equation or, more specifically, the equation of the ellipse.

By applying (5), the Cartesian form for the equation of the bus ellipse is defined as (4) [19].

$$\sin^2(\omega t) + \cos^2(\omega t) = 1 \tag{3}$$

$$x^2(t) - 2\cos(\phi)\, x(t)\, y(t) + y^2(t) - \sin^2(\phi) = 0 \tag{4}$$

$$x(t) = \frac{u(t)}{U_0} = \sin(\omega t) \tag{5}$$

$$y(t) = \frac{i(t)}{I_0} = \sin(\omega t - \phi) \tag{6}$$

The equation of the ellipse, for any value of U_0 and I_0, is given by

$$\begin{aligned} I_0^2 u^2(t) - 2U_0 I_0 \cos(\phi)\, u(t)\, i(t) + U_0^2 i^2(t) \\ - U_0^2 I_0^2 \sin^2(\phi) = 0 \end{aligned} \tag{7}$$

Hence, as for a bus, using the geometric properties of (7) can monitor the behavior of voltage and current signals for each phase and identify the moment when potential faults have occurred; besides, this paper proposes that the parameters of the ellipse can be seen as an index to indicate the faulty section location, which is elaborated in the following sections.

2.2. Feature Cosine. According to [20], an ellipse section defined in R^2 represents a set of points whose coordinates satisfy the general equation (8), the form of (8) is equivalent to (7), and (8) can be seen as a fitting model to obtain the parameters of (7).

$$ax^2 + bxy + cy^2 + dx + ey + f = 0 \tag{8}$$

with the parameters a or b or $c \neq 0$.

Then, (7) and (8) can both be rewritten in matrix form as

$$f(\boldsymbol{x}) = \boldsymbol{\alpha x} + 1 \tag{9}$$

$$\begin{aligned} \boldsymbol{a} &= [a \;\; b \;\; c \;\; d \;\; e] \\ \boldsymbol{x} &= [x_1 \;\; x_2 \;\; x_3 \;\; x_4 \;\; x_5]^{\mathrm{T}} = [x^2 \;\; xy \;\; y^2 \;\; x \;\; y]^{\mathrm{T}} \\ &= [u^2(t) \;\; u(t)\, i(t) \;\; i^2(t) \;\; u(t) \;\; i(t)]^{\mathrm{T}} \end{aligned} \tag{10}$$

Based on the minimum least squares, a cost function J_a can be written as

$$J_a(a, \cdots, e) = \frac{1}{2}\sum_{i=1}^{n} [f(\boldsymbol{x}_i) - 0]^2 \tag{11}$$

Hence, the parameters estimation problem is transformed into a simpler problem of finding a local minimizer for J_a; this problem can be solved by Levenberg-Marquardt algorithm, and it is described in [16, 17].

Lastly, the parameters of equation (7) can be obtained from Levenberg-Marquardt algorithm.

$$\boldsymbol{a} = \boldsymbol{a}^* = [a^* \;\; b^* \;\; c^* \;\; d^* \;\; e^*] \tag{12}$$

And the feature cosine $\cos(\phi)$ can be shown in (13), $\cos(\phi)$ can represent the phase relation between the voltage and current, and it is mentioned that $\cos(\phi)$ for each phase is a constant even in the condition of unbalanced loads if a microgrid operates normally. $\cos(\phi)$ is the index mentioned in Section 2.1. Section 3 will illustrate why $\cos(\phi)$ can be employed to detect microgrid faulty location.

$$\cos(\phi) = -\frac{b^*}{\left(2\sqrt{a^*} \cdot \sqrt{c^*}\right)} \tag{13}$$

3. Feature Cosine Utilization Reason

3.1. Microgrid Topology. A modified microgrid based on the topology of CERTS microgrid model [21] is shown in Figure 2(a) and established in Matlab/Simulink. This microgrid is a part of the power distribution system, and it is connected to the utility grid using a transformer 0.4/10kV. Each distributed generation (DG) is controlled by improved droop controller [22, 23]. Table 1 shows each load capacity. The system parameters are given: the power electronic device is the IGBT; the capacities of DGs are all 80kVA; switch frequency is 6kHz; the DC voltage is 800V; Line: resistance and inductance are 0.642 Ω/km and 0.083H/km; the length of Line 1, Line 2, and Line 3 are 0.3km, 0.2km, and 0.5km, respectively.

3.2. Reason. The fault current-limiting strategy is applied for each DG according to [24, 25]. For example, when the microgrid occurs, three-line-ground (LLLG) fault or single-line-ground (LG) fault at 0.2s, whose faulty location is Line 2 of Figures 2(a), 2(b), and 2(c), shows that the fault current-limiting strategy, after 0.21s, can effectively limit each DG fault current into 2 times of the rated current; besides, this strategy can restrain the harmonics and make the frequency of output current and voltage equal to 50Hz. This is the reason why this paper can use the feature cosine to detect the faulty section.

4. The Analysis of Microgrid Fault Feature

4.1. Fault at Line 1. Based on the analysis method from [26], this paper focuses on the current direction. When short-circuit fault occurs at Line 1 of Figure 2(a), B_1, B_2, B_3, B_4, and B_5 are bus. Taking B_1 and B_2 as an example, Figure 3 shows the current direction of B_1 and B_2, which is suitable for the islanded mode and grid connected mode.

When DGs supply power for downstream load shown in Figure 3(a), phase ϕ_1 and ϕ_2 are shown in (14); this is because loads in microgrid are generally inductive loads.

$$\begin{aligned} \phi_1 &= \arg\left(\dot{U}_1\right) - \arg\left(\dot{I}_1\right) > 0^\circ \\ \phi_2 &= \arg\left(\dot{U}_2\right) - \arg\left(\dot{I}_2\right) > 0^\circ \end{aligned} \tag{14}$$

where $\dot{U}_1$ and $\dot{U}_2$ are the voltage of B_1 and B_2. $\dot{I}_1$ and $\dot{I}_2$ are the current of B_1 and B_2. $\arg(\dot{U}_1)$ means the voltage phase of B_1. $\arg(\dot{I}_1)$ means the current phase of B_1.

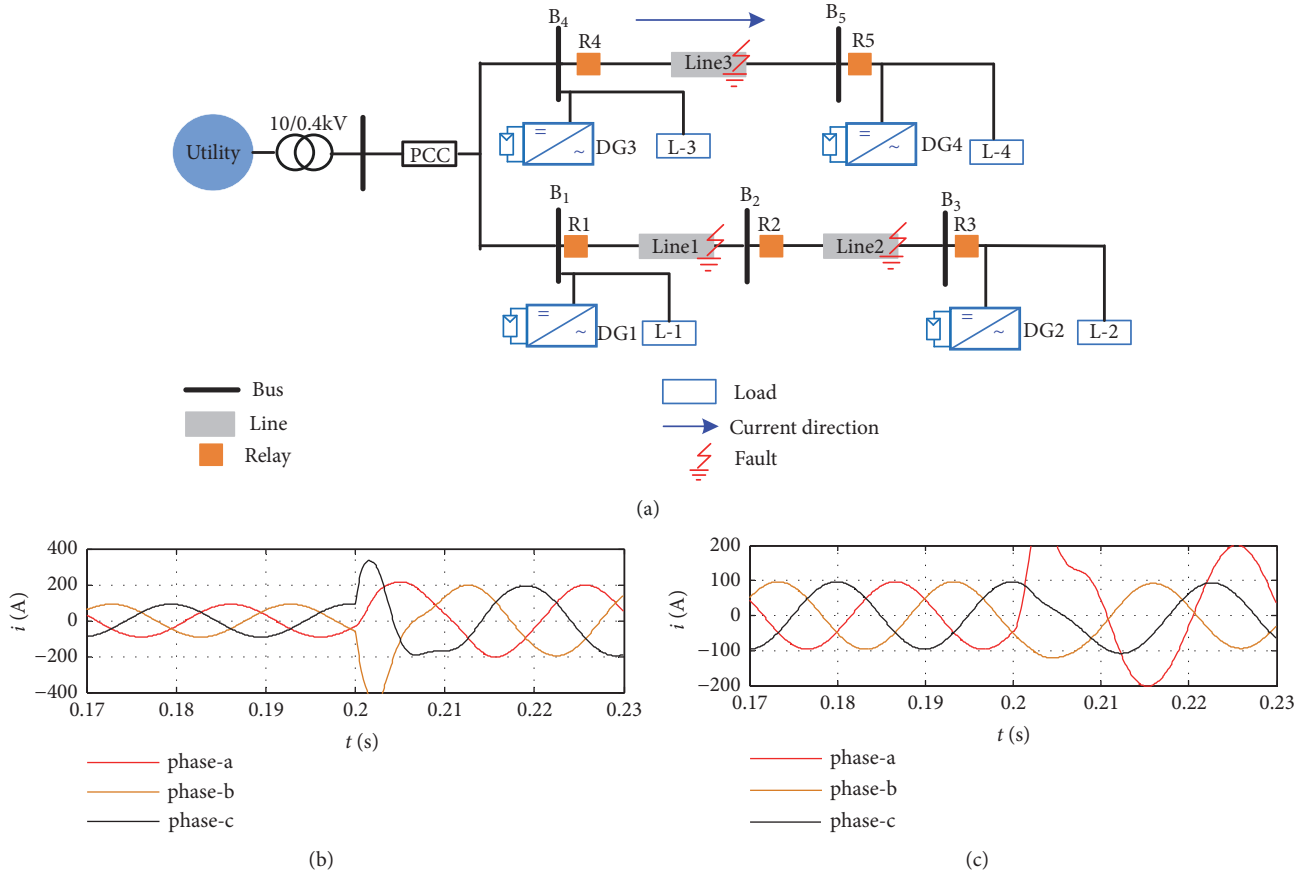

FIGURE 2: Single line diagram and fault current of microgrid. (a) Single line diagram; (b) fault current by DG1 at LLLG; (c) fault current by DG2 at LG.

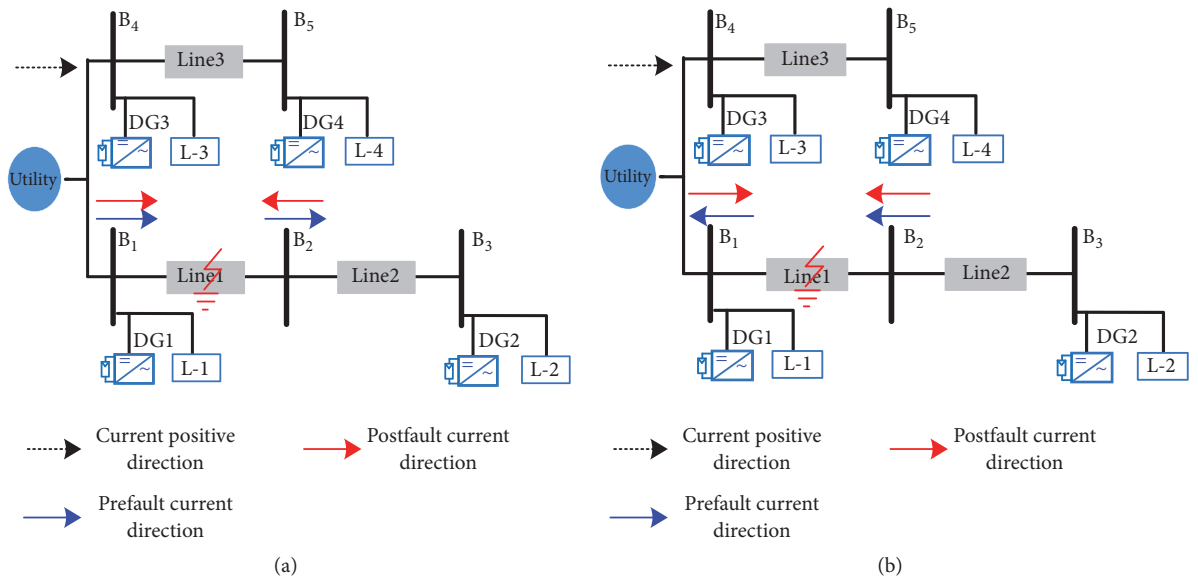

FIGURE 3: The current direction of B_1 and B_2 when fault occurs at Line 1. (a) DGs supply power for downstream load; (b) DGs supply power for upstream load.

Table 1: The capacity of loads.

Load Name	Active power in kW	Reactive power in kVar
L-1	45	15
L-2	45	22.5
L-3	35	10
L-4	45	15

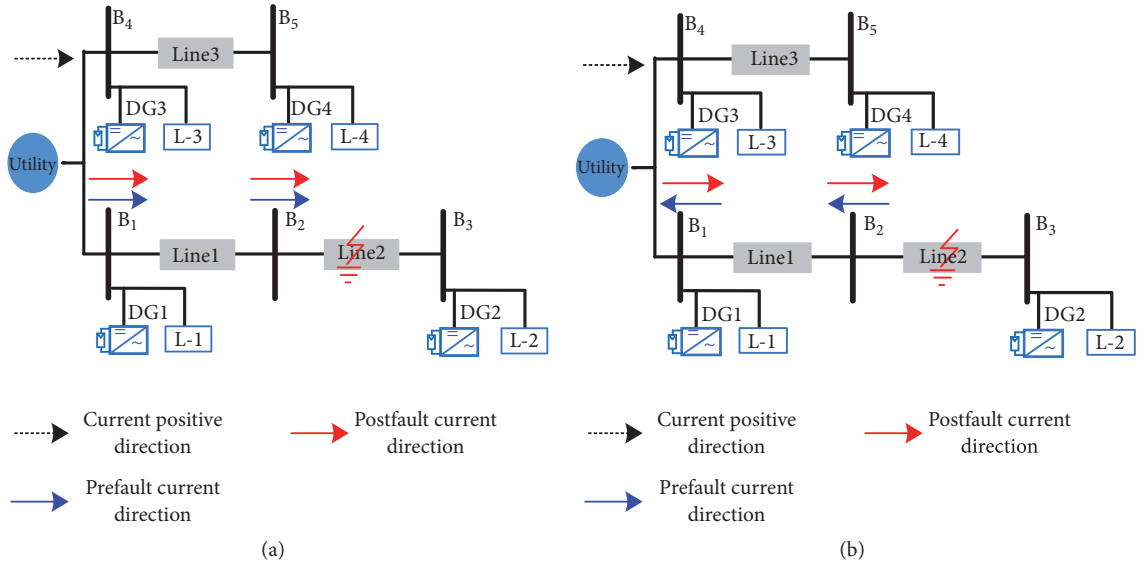

Figure 4: The current direction of B_1 and B_2 when fault occurs at Line 2. (a) DGs supply power for downstream load; (b) DGs supply power for upstream load.

After fault, because the grounding impedance of fault point is obviously less than the load impedance [22], as for current direction, B_1 and B_2 are both from bus to fault point. Moreover, the voltage phases of B_1 and B_2 are not changed. Based on this, (15) and (16) can be expressed and present that $\cos(\phi_1^f)$ is positive and $\cos(\phi_2^f)$ is negative when the fault occurs at Line 1.

$$\begin{aligned}\phi_1^f &= \arg\left(\dot{U}_1^f\right) - \arg\left(\dot{I}_1^f\right) \approx \arg\left(\dot{U}_1\right) - \arg\left(\dot{I}_1\right) \\ &> 0^\circ \\ \phi_2^f &= \arg\left(\dot{U}_2^f\right) - \arg\left(\dot{I}_2^f\right) \\ &\approx \arg\left(\dot{U}_2\right) - \arg\left(\dot{I}_2\right) - 180^\circ < -90^\circ\end{aligned} \tag{15}$$

$$\begin{aligned}\cos\left(\phi_1^f\right) &\approx \cos\left(\arg\left(\dot{U}_1\right) - \arg\left(\dot{I}_1\right)\right) > 0 \\ \cos\left(\phi_2^f\right) &\approx \cos\left(\arg\left(\dot{U}_2\right) - \arg\left(\dot{I}_2\right) - 180^\circ\right) < 0\end{aligned} \tag{16}$$

where ϕ_1^f and (ϕ_2^f) are the postfault phase of B_1 and B_2.

When the DGs supply power for upstream load, the current directions at B_1 and B_2 are shown in Figure 3(b). Through analyzing, when the fault occurs at Line 1, $\cos(\phi_1^f)$ is positive and $\cos(\phi_2^f)$ is negative.

4.2. Fault at Line 2. When the fault occurs at Line 2 of Figure 2(a), the current direction of B_1 and B_2 is shown in Figure 4.

When the DGs supply power for downstream loads shown in Figure 4(a) and the fault occurs at Line 2, the current directions, the current directions of B_1 and B_2 are both from bus to fault point because the load impedance is bigger than the grounding impedance [22]. $\cos(\phi_1^f)$ and $\cos(\phi_2^f)$ can be shown in

$$\begin{aligned}\cos\left(\phi_1^f\right) &\approx \cos\left(\arg\left(\dot{U}_1\right) - \arg\left(\dot{I}_1\right)\right) > 0 \\ \cos\left(\phi_2^f\right) &\approx \cos\left(\arg\left(\dot{U}_2\right) - \arg\left(\dot{I}_2\right)\right) > 0\end{aligned} \tag{17}$$

Similarly, if the DGs supply power for downstream load shown in Figure 4(b), $\cos(\phi_1^f)$ and $\cos(\phi_2^f)$ are both positive when fault occurs at Line 2.

4.3. Fault at Line 3. The current direction of B_1 and B_2 is shown in Figure 5 when the fault occurs at Line 3 of Figure 2(a). There are two situations as follows because the distance is relatively far from fault point to B_2.

(I) The grounding impedance is relatively small; that is, the effect of fault point on B_2 is serious. And the current direction of B_1 and B_2 will be both from bus to fault point; these directions are opposite to that in prefault and are shown

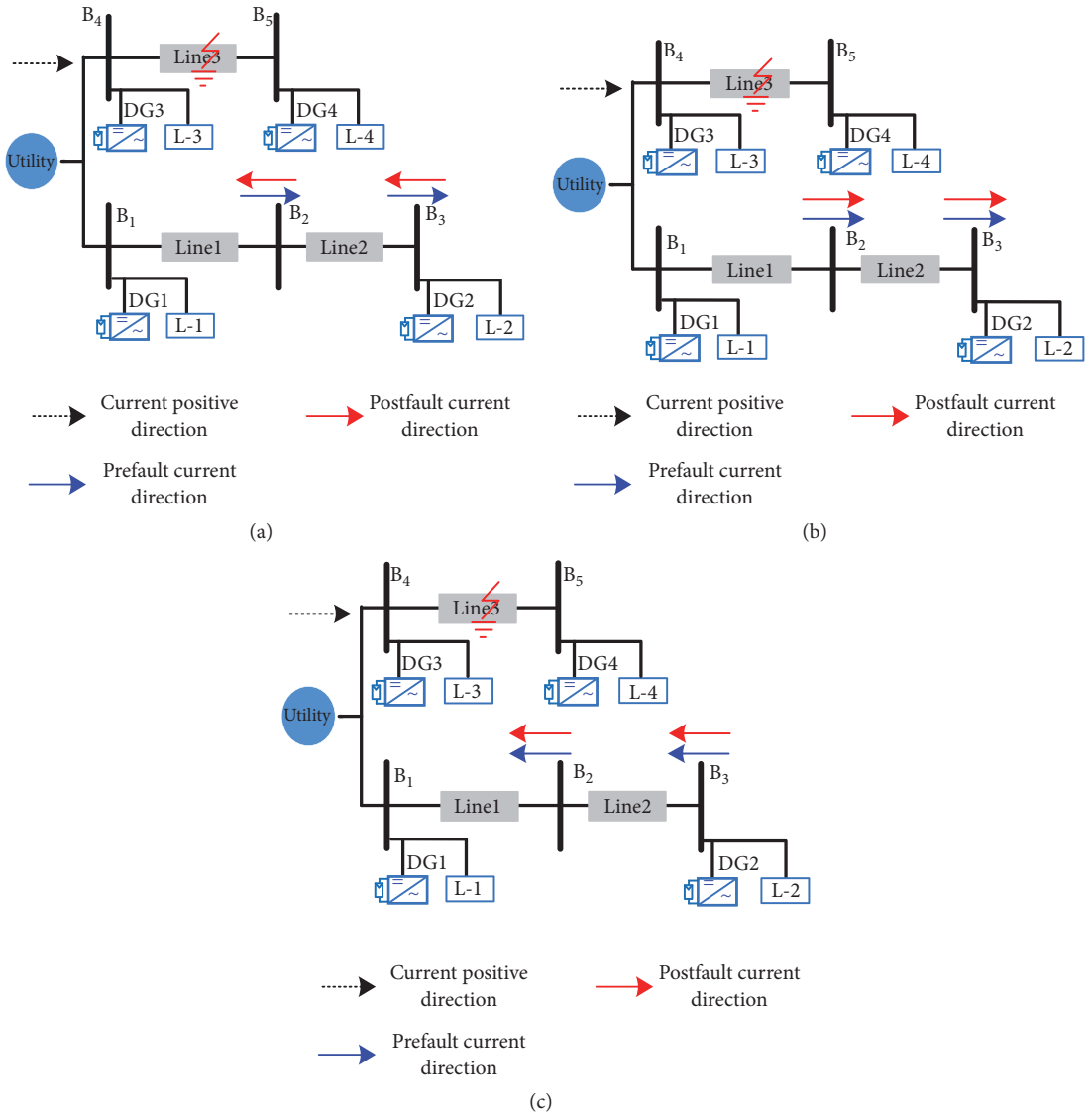

Figure 5: The current direction of B_1 and B_2 when fault occurs at Line 3. (a) DGs supply power for downstream load when the effect is serious; (b) DGs supply power for downstream load when the effect is mild; (c) DGs supply power for upstream load.

in Figure 5(a). (18) shows their feature cosine; they are both negative.

$$\cos\left(\phi_1^{\mathrm{f}}\right) \approx \cos\left(\arg\left(\dot{U}_1\right) - \arg\left(\dot{I}_1\right) - 180^{\circ}\right) < 0$$
$$\cos\left(\phi_2^{\mathrm{f}}\right) \approx \cos\left(\arg\left(\dot{U}_2\right) - \arg\left(\dot{I}_2\right) - 180^{\circ}\right) < 0 \quad (18)$$

(II) When the effect of fault point on B_2 is mild, the current direction of B_1 and B_2 can be maintained; these are same as that in prefault shown in Figure 5(b). The $\cos(\phi_1^{\mathrm{f}})$ and $\cos(\phi_2^{\mathrm{f}})$ are both positive.

Similarly, if the DGs supply power for upstream load shown in Figure 5(c), there are also two situations according to the effect of fault point on B_2. And $\cos(\phi_1^{\mathrm{f}})$ and $\cos(\phi_2^{\mathrm{f}})$ will be both negative in these two situations.

In summary, no matter how the initial current direction changes in bus, $\cos(\phi_1^{\mathrm{f}})$ is positive and $\cos(\phi_2^{\mathrm{f}})$ is negative when the fault occurs at the section between B_1 and B_2. Moreover, there are two situations when the fault does not occur at the area between B_1 and B_2: (1) $\cos(\phi_1^{\mathrm{f}})$ and $\cos(\phi_2^{\mathrm{f}})$ are both positive and (2) $\cos(\phi_1^{\mathrm{f}})$ and $\cos(\phi_2^{\mathrm{f}})$ are both negative. These can be clearly shown in Table 2 where "+" is positive, "−" is negative. The difference of feature cosine can be utilized to detect the faulty section in the next section.

5. Protection Methodology

Firstly, it is mentioned that the relays at the ends of a bus are considered and not at the ends of the line; this is because it can reduce the number of relays being used; however, the circuit breakers need to be installed at the ends of the line for isolating a fault.

Table 2: The direction of feature cosine of B_1 and B_2.

Faulty part	B_1	B_2
Line1	+	−
Line2	+	+
	−	−
Line3	+	+
	−	−

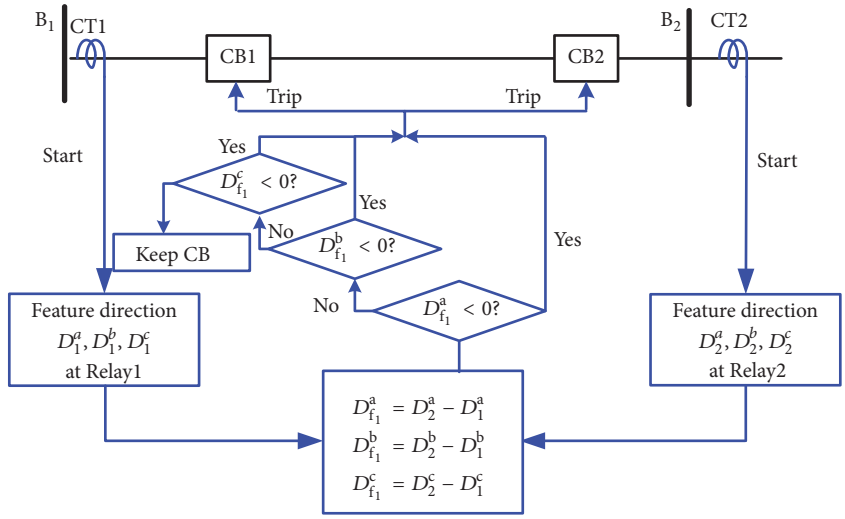

Figure 6: The procedures of this paper's proposed method.

Then, it is presented how to obtain the feature direction (D) of each bus through feature cosine.

Step 1. $u^w_n(t), u^w_{n+1}(t), i^w_n(t)$, and $i^w_{n+1}(t)$ are retrieved at B_n and B_{n+1}, $u^w_n(t)$ and $i^w_n(t)$ are the normalized voltage and current of phase-w of B_n, $u^w_{n+1}(t)$ and $i^w_{n+1}(t)$ are the normalized voltage and current of phase-w of B_{n+1}, w is a or b or c, n is the number of bus, and n is equal to 1, 2 and 4.

Step 2. As for B_n, according to Levenberg-Marquardt algorithm, the parameters of bus ellipse equation $\boldsymbol{\alpha}^w_n$ can be calculated. $\boldsymbol{\alpha}^w_n$ can represent the behavior of voltage and current signals.

$$\boldsymbol{a}^w_n = \left[a^w_n \;\; b^w_n \;\; c^w_n \;\; d^w_n \;\; e^w_n\right] \tag{19}$$

Step 3. Similarly, as for B_{n+1}, the parameters of line ellipse equation $\boldsymbol{a}^w_{n+1}$ can be obtained.

$$\boldsymbol{a}^w_{n+1} = \left[a^w_{n+1} \;\; b^w_{n+1} \;\; c^w_{n+1} \;\; d^w_{n+1} \;\; e^w_{n+1}\right] \tag{20}$$

Step 4. $\cos(\phi^w_n)$ and $\cos(\phi^w_{n+1})$ are calculated, $\cos(\phi^w_n)$ and $\cos(\phi^w_{n+1})$ are the feature cosine of B_n and B_{n+1}.

$$\cos\left(\phi^w_n\right) = -\frac{b^w_n}{\left(2\sqrt{a^w_n}\sqrt{c^w_n}\right)} \tag{21}$$

$$\cos\left(\phi^w_{n+1}\right) = -\frac{b^w_{n+1}}{\left(2\sqrt{a^w_{n+1}}\sqrt{c^w_{n+1}}\right)} \tag{22}$$

Step 5. D^w_n, D^w_{n+1}, and D^w_{cn} can be obtained by the following equations. D^w_n and D^w_{n+1}, which can show the fault current direction of bus, are the feature direction of B_n and B_{n+1}, and D^w_{cn} is the differential direction.

$$D^w_n = \begin{cases} 1, & \cos\left(\phi^w_n\right) > 0 \\ -1, & \cos\left(\phi^w_n\right) < 0, \end{cases}$$
$$D^w_{n+1} = \begin{cases} 1, & \cos\left(\phi^w_{n+1}\right) > 0 \\ -1, & \cos\left(\phi^w_{n+1}\right) < 0 \end{cases} \tag{23}$$

$$D^w_{cn} = D^w_{n+1} - D^w_n \tag{24}$$

Lastly, if $D^w_{cn} < 0$, the section between B_n and B_{n+1} is judged as faulty section; if $D^w_{cn} \geqq 0$, the section between B_n and B_{n+1} is judged as healthy section. Taking B_1 and B_2 as an example, the procedures of this paper's proposed method can be shown clearly in Figure 6.

6. Simulation Results

In order to prove the effectiveness of the proposed method in this paper, different fault conditions are simulated through Matlab/Simulink for the microgrid shown in Figure 2(a), and conditions for the fault study are explained as follows.

(1) Faulty resistances (R_f): 0.01, 0.1, 0.2, 0.3, 0.5, 1, 5, 10 Ω.

Table 3: The feature cosine of each bus and results with different grounding resistances.

R_f	P	[B_1, B_2, B_3, B_4, B_5]	Each P result	Final result
0.01Ω	a	[0.954, -0.990, -0.982, -0.859, -0.729]	B_1- B_2	B_1-B_2
	b	[0.998, 0.999, 0.999, -1.007, -1.009]	healthy	
	c	[0.999, 0.999, 0.999, -0.997, -0.995]	healthy	
0.1Ω	a	[0.961, -0.986, -0.978, -0.904, -0.797]	B_1 - B_2	B_1-B_2
	b	[0.998, 0.998, 0.998, -0.991, -0.987]	healthy	
	c	[0.998, 0.998, 0.999, -0.992, -0.989]	healthy	
0.5Ω	a	[0.999, -1.000, -0.999, -0.997, -0.997]	B_1 - B_2	B_1 - B_2
	b	[-0.891, -0.894, -0.896, 0.720, 0.699]	healthy	
	c	[-0.958, -0.960, -0.962, 0.925, 0.919]	healthy	
2Ω	a	[0.936, -0.979, -0.960, -0.897, -0.767]	B_1 - B_2	B_1-B_2
	b	[0.999, 0.999, 1.000, -0.994, -0.993]	healthy	
	c	[1.000, 1.000, 1.001, -0.996, -0.994]	healthy	
10Ω	a	[0.927, -0.974, -0.952, -0.888, -0.752]	B_1 - B_2	B_1-B_2
	b	[0.999, 0.999, 0.999, -0.995, -0.993]	healthy	
	c	[0.999, 0.999, 1.000, -0.998, -0.997]	healthy	

(2) Different faulty types (F_t): single-line-ground (LG), double-line-ground (LLG), line-line (LL), and three-line-ground (LLLG), where LG(a) means the single-line-ground whose faulty phase is phase-a.

(3) Faulty section (F_L): Line 1, Line 2, and Line 3.

(4) Different microgrid operation modes (O_m): islanded and grid connected mode.

(5) Unbalanced loads: each phase capacity of load is changed.

(6) Noise influence: the signal to noise ratio (SNR) is set as 50db, 20db, and 5db.

6.1. Different Grounding Resistances. When the microgrid shown in Figure 2(a) is operated in islanded mode, LG fault is supposed to happen in Line 1 at $t = 0.2$s; that is, faulty section is between B_1 and B_2 labelled B_1-B_2. Faulty conditions include that faulty phase is phase-a and grounding resistances are set to 0.01Ω, 0.5Ω, 0.1Ω, 2Ω, and 10Ω, respectively. Then Table 3 gives the feature cosine of each bus and judgment results after implementing this paper's method; P is phase sequence.

Take grounding resistance 0.5Ω as an example, Figure 7 gives the voltage and current of B_1 and B_2, and Figure 8 shows the bus ellipses of each phase of B_1 and B_2. Figure 7 illustrates that the faulty phase voltage direction of B_1 is same as that of B_2 and the faulty phase current direction of B_1 is opposite to that of B_2, which is illustrated obviously in Figure 8.

Then, as for phase-a, from Table 3 and this paper's method, the feature cosines from B_1 to B_5 are 0.999, -1.000, -0.999, -0.997, and -0.997, respectively. So, the feature directions from B_1 to B_5 are 1, -1, -1, -1, and -1, respectively; that is, their differential directions are -2, 0, 0, 0, respectively. Similarly, as for phase-b and phase-c, their differential directions are all 0. Hence, the faulty section is between B_1 and B_2; this result is consistent with the actual fault. Lastly, from Table 3 we can find that this paper's method can detect fault part effectively in different grounding resistances.

6.2. Different Faulty Types. When the microgrid is operated in islanded mode, different faulty types, including LG(b), LLG(ab), LL(bc), and LLLG, are supposed to happen in Line 1 at 0.2s with grounding resistance 0.1Ω; that is, faulty section is B_1-B_2. Then, Table 4 gives the feature cosine of each bus and judgment results; it shows that the proposed method cannot be influenced by different faulty types.

6.3. Different Faulty Section Locations. The islanded microgrids are simulated at 0.2s with different faulty section locations, including B_1-B_2, B_2-B_3, and B_4-B_5. The fault conditions include fault type LG whose faulty phase is phase-c or phase-a; grounding resistances is 0.3Ω or 10Ω. Then, Table 5 illustrates that this paper's method can detect different fault parts. It is mentioned that the feature cosine is consist with the analysis in Section 4.3 when the grounding resistance is 10Ω and faulty section location is B_4-B_5.

6.4. Grid Connected Operation Mode. When the microgrid is operated at grid connected mode, different faults are supposed to happen including different faulty section locations, types, and grounding resistances. Table 6 gives the judgments and shows that this paper's method can detect different faults in grid connected operation mode; besides, the protection scheme cannot be changed compared with islanded mode.

6.5. Unbalanced Loads. In order to prove the effectiveness of proposed method in the condition of the unbalanced loads, the capacity of load L-2 in Figure 2(a) is set as follows: phase-a: the active power and reactive power are 19kW and 8kW; phase-b: the active power and reactive power are 17kW and

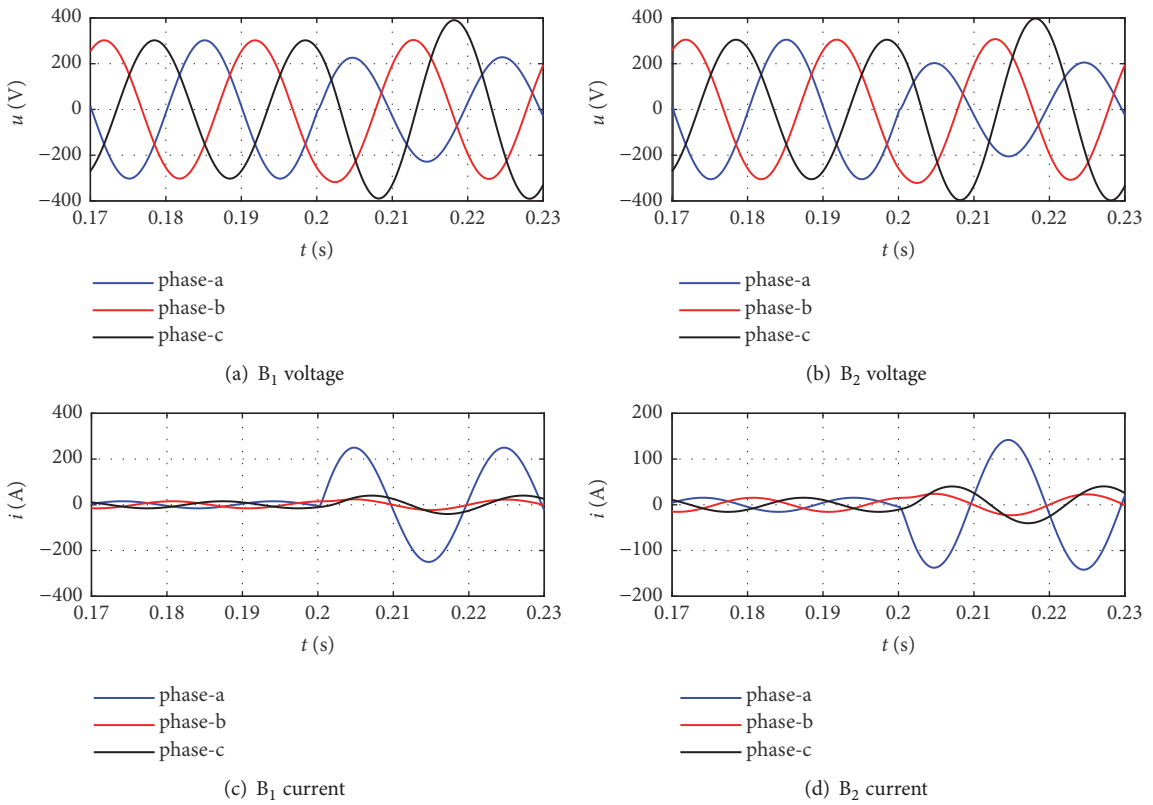

FIGURE 7: The voltage and current of B_1 and B_2 when fault occurs at Line 1. (a) B_1 voltage; (b) B_2 voltage; (c) B_1 current; (d) B_2 current.

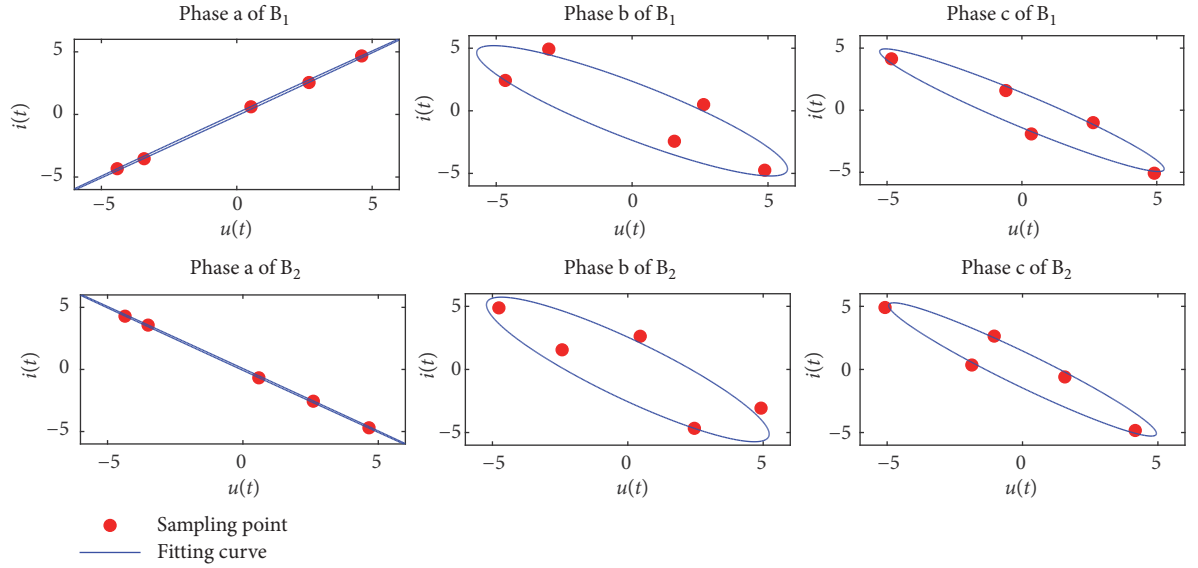

FIGURE 8: The bus ellipse of B_1 and B_2 for different phases. (a) Phase-a; (b) phase-b; (c) phase-c.

7kW; phase-c: the active power and reactive power are 10kW and 8kW.

When different faults are supposed to happen in the microgrid, Table 7 gives the feature cosine of each bus and judgment results. When faulty condition is that faulty section location is B_1-B_2, grounding resistance is 0.1Ω, operation mode is islanded, and faulty type is LG (a), Figure 9 is the current of B_2 and the bus ellipses of B_1 and B_2. From Figure 9 and Table 7, this paper method can achieve the faulty section location detection in the condition of the unbalanced loads.

Table 4: The feature cosine of each bus and judgment results with different faulty types.

F_t	P	[B_1, B_2, B_3, B_4, B_5]	Each P result	Final result
LG (b)	a	[1.003, 1.003, 1.003, -1.008, -1.012]	healthy	B_1-B_2
	b	[0.928, -0.915, -0.871, -1.100, -1.084]	B_1-B_2	
	c	[1.002, 1.002, 1.002, -0.991, -0.9867]	B_1-B_2	
LLG (ab)	a	[0.957, -0.946, -0.915, -0.994, -0.970]	B_1-B_2	B_1-B_2
	b	[0.672, -0.508, -0.380, -0.829, -0.614]	B_1-B_2	
	c	[0.998, 0.997, 0.997, 1.004, 1.006]	healthy	
LL (bc)	a	[0.401, 0.631, 0.715, 0.113, 0.897]	healthy	B_1-B_2
	b	[0.953, -0.941, -0.958, -0.977, -0.900]	B_1-B_2	
	c	[0.956, -0.943, -0.957, -0.978, -0.909]	B_1-B_2	
LLL	a	[0.836, -0.636, -0.473, -0.949, -0.869]	B_1-B_2	B_1-B_2
	b	[0.609, -0.696, -0.497, -0.852, -0.642]	B_1-B_2	
	c	[0.999, -0.866, -0.770, -1.040, -1.010]	B_1-B_2	

Table 5: The feature cosine of each bus and judgment results in different faulty section locations.

F_t R_f F_L	P	[B_1, B_2, B_3, B_4, B_5]	Each P result	Final result
LG(c)	a	[0.998, 0.999, 0.999, -0.988, -0.985]	healthy	B_1-B_2
0.3Ω	b	[0.998, 0.999, 0.999, -0.990, -0.987]	healthy	
B_1-B_2	c	[0.883, -0.940, -0.906, -0.797, -0.656]	B_1-B_2	
LG(c)	a	[0.985, 0.990, 0.992, -0.972, -0.963]	healthy	B_2-B_3
0.3Ω	b	[0.988, 0.992, 0.993, -0.974, -0.965]	healthy	
B_2-B_3	c	[0.766, 0.922, -0.979, -0.739, -0.627]	B_2-B_3	
LG(c)	a	[-0.821, -0.806, -0.796, 0.835, 0.850]	healthy	B_4-B_5
0.3Ω	b	[-0.847, -0.833, -0.825, 0.847, 0.861]	healthy	
B_4-B_5	c	[-0.618, -0.472, -0.374, 0.866, -0.9461]	B_4-B_5	
LG(a)	a	[0.909, -0.956, -0.922, -0.525, -0.345]	B_1-B_2	B_1-B_2
10Ω	b	[0.998, 0.998, 0.998, -0.996, -0.994]	healthy	
B_1-B_2	c	[0.999, 1.000, 1.000, -0.993, -0.992]	healthy	
LG(a)	a	[0.544, 0.780, -0.993, -0.486, -0.324]	B_2-B_3	B_2-B_3
10Ω	b	[0.993, 0.995, 0.996, -0.985, -0.980]	healthy	
B_2-B_3	c	[0.994, 0.996, 0.997, -0.992, -0.989]	healthy	
LG(a)	a	[-0.210, -0.105, -0.034, 0.795, -0.985]	B_4-B_5	B_4-B_5
10Ω	b	[-0.923, -0.909, -0.899, 0.942, 0.953]	healthy	
B_4-B_5	c	[-0.922, -0.910, -0.899, 0.931, 0.939]	healthy	

6.6. Noise Influence. In fact, the elliptical representation of the behavior of both voltage and current signals should consider the existence of the noise, which is inherent in the processes of generation, transmission, or even disturbances related to digital recorders. Hence, in order to implement the proposed method effectively, the wavelet denoising method is employed [27]. It is embedded in Step 1 of Section 5.

When different faults with different SNR including 50db and 5db are supposed to happen in the microgrid, Table 8 shows that this paper method after adding wavelet denoising method can detect faulty section locations in different SNR including 50db and 5db.

6.7. Looped Microgrid. When different faults are supposed to happen in the looped microgrid shown in Figure 10, Table 9 gives the feature cosine of each bus and judgment results. From Table 9, we can know that this paper method can achieve the faulty section location detection in different faulty conditions for looped microgrid.

6.8. Sample Microgrid. When different faults are supposed to happen in the looped microgrid shown in Figure 11, Table 10 gives the feature cosine of each bus and judgment results. From Table 10, we can know that this paper method can

Table 6: The feature cosine of each bus and judgment results in grid connected operation mode.

F_t R_f F_L	P	[B_1, B_2, B_3, B_4, B_5]	Each P result	Final result
LG(a)	a	[0.054, -0.540, -0.271, -0.985, -0.974]	B_1-B_2	B_1-B_2
0.01Ω	b	[-0.5926, 1.000, 1.000, 0.4800, 0.340]	healthy	
B_1-B_2	c	[-0.443, -0.013, 0.842, 0.256, 0.421]	healthy	
LG(b)	a	[0.191, 0.780, 0.901, 0.768, 0.822]	healthy	B_1-B_2
0.2Ω	b	[0.507, -0.909, -0.840, -0.984, -0.981]	B_1-B_2	
B_1-B_2	c	[0.181, 0.764, 0.895, 0.713, 0.782]	healthy	
LLG(ac)	a	[0.107, 0.999, -0.829, -0.656, -0.021]	B_2-B_3	B_2-B_3
0.5Ω	b	[0.112, 0.875, 0.940, 0.709, 0.759]	healthy	
B_2-B_3	c	[0.108, 0.989, -0.839, -0.899, -0.545]	B_2-B_3	
LLG(bc)	a	[-0.559, 0.856, 0.943, -0.005, 0.228]	B_2-B_3	B_2-B_3
5Ω	b	[0.649, 0.974, -0.701, -0.967, -0.431]	B_2-B_3	
B_2-B_3	c	[0.637, 0.973, -0.749, -0.961,0.307]	healthy	
LLL	a	[-0.948, -0.870, -0.585, 0.053, -0.319]	B_4-B_5	B_4-B_5
10Ω	b	[-0.935, -0.843, -0.515, 0.619, -0.302]	B_4-B_5	
B_4-B_5	c	[-0.987, -0.969, -0.193, 0.575, -0.515]	B_4-B_5	

Table 7: The feature cosine of each bus and judgment results in unbalanced loads.

F_t R_f F_L O_m	P	[B_1, B_2, B_3, B_4, B_5]	Each P result	Final result
LG(a)	a	[-0.999, 0.999, 0.999, 0.995, 0.997]	B_1-B_2	B_1-B_2
0.1Ω	b	[0.653, 0.667, 0.675, -0.867, -0.851]	healthy	
B_1-B_2 islanded	c	[0.840, 0.852, 0.859, -0.911, -0.902]	healthy	
LL(ab)	a	[-0.969, -0.834, 0.948, 0.951, 0.984]	B_2-B_3	B_2-B_3
0.1Ω	b	[-0.718, -0.043, -0.856, 0.909, 0.931]	healthy	
B_2-B_3 islanded	c	[0.948, 0.949, 0.949, -0.999, -0.998]	B_2-B_3	
LLLG	a	[0.994, 0.999, 1.000, -0.991, 0.985]	B_4-B_5	B_4-B_5
0.1Ω	b	[0.936, 0.979, 0.987, -1.021, 1.095]	B_4-B_5	
B_4-B_5 islanded	c	[1.095, 1.023, 1.006, -0.991, 0.966]	B_4-B_5	
LG(b)	a	[-0.167, -0.191, -0.208, 0.115, 0.109]	healthy	B_1-B_2
1Ω	b	[0.999, -0.980, -0.980, -0.137, -0.169]	B_1-B_2	
B_1-B_2 Grid	c	[-0.774, -0.780, -0.785, -0.296, -0.298]	healthy	
LLG(ab)	a	[0.958, 0.735, -0.921, -0.456, -0.557]	B_2-B_3	B_2-B_3
1Ω	b	[0.837, 0.341, 0.798, -0.993, -0.997]	healthy	
Grid B_2-B_3	c	[-0.960, -0.961, -0.962, 0.588, 0.582]	healthy	
LLLG	a	[-0.836, -0.880, -0.899, 0.997, -0.994]	B_4-B_5	B_4-B_5
1Ω	b	[-0.840, -0.887, -0.912, 0.993, -1.038]	B_4-B_5	
Grid B_4-B_5	c	[-0.933, -0.952, -0.964, 0.994, -0.899]	B_4-B_5	

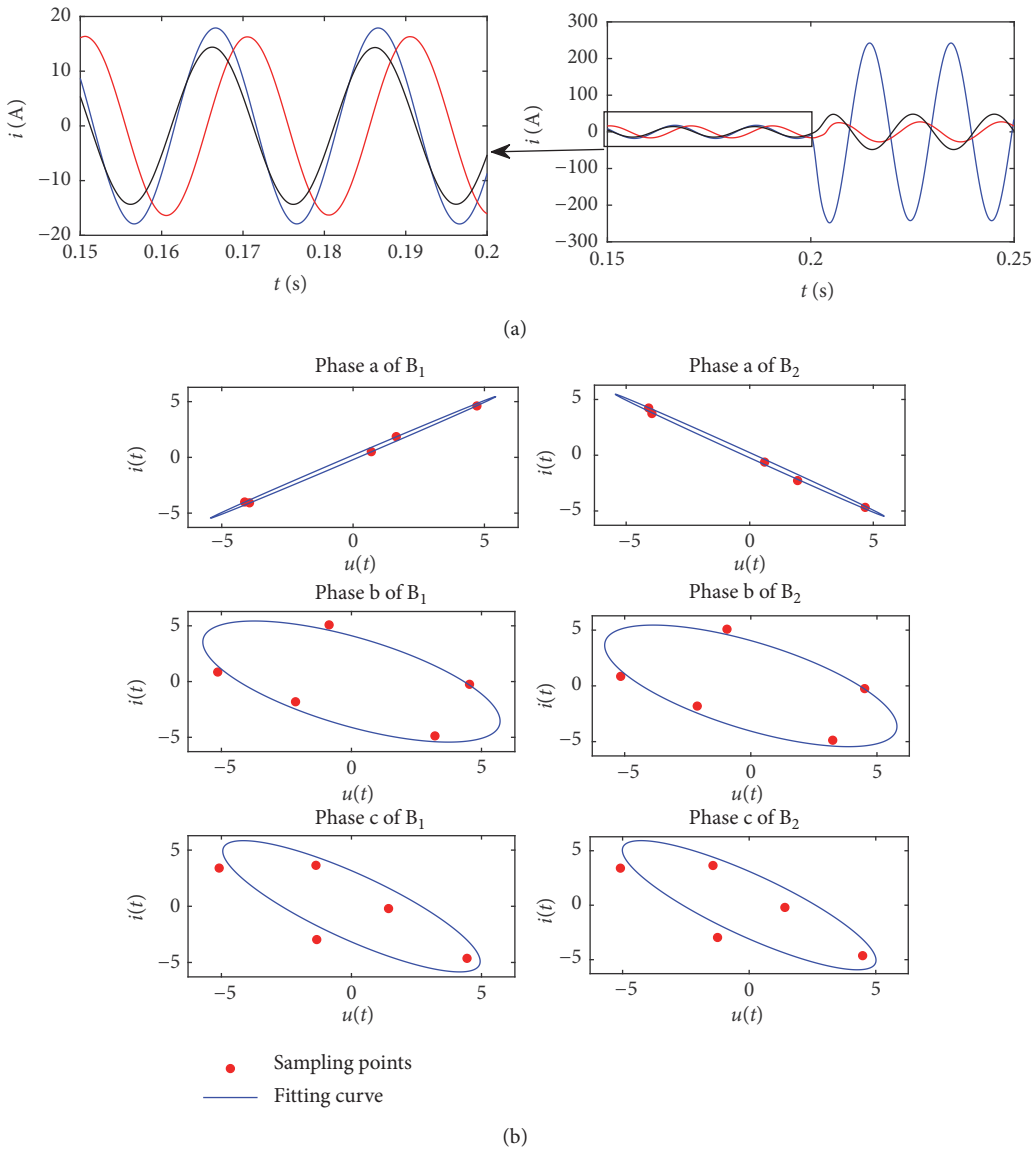

Figure 9: The B_2 current and bus ellipse for B_1 and B_2; (a) B_2 current, (b) bus ellipse of three phases.

achieve the faulty section location detection in different faulty conditions for the microgrid whose nodes are with only loads.

7. Discussion

When different faults, including different faulty resistances and faulty section, occur in microgrid at 0.2s, Figure 12 shows the fault current peak value of B_1 whose time length is from 0.21s~0.23s.

It is shown in Figure 10 that the B_1 fault current in grid connected mode is higher compared with the islanded mode; besides, the B_1 fault current decreases for the faults occurring on the lines away from the B_1. So, as for fault current, there is a difference between grid connected and islanded modes; besides, if the microgrid has unbalanced loads, its fault current for each phase is obviously different. It can be concluded that most commercially used overcurrent relay with a preset threshold to operate in grid connected mode may fail or may take a longer time to operate in islanded mode [2]. Hence, [14] has different thresholds to detect fault when the microgrid is operated in different modes. However, [14] did not consider the condition of unbalanced load and will make the protection scheme more complex. Hence, in this paper, the protection method, which has the same threshold in different operation mode and unbalanced load, is proposed and superior to [14].

8. Conclusion

Based on the geometric representation of one phase in a bus and the analysis of feature cosine of different buses, this paper proposes a protection method to detect the faulty section location using the differential direction. The proposed method uses comprehensively every phase voltage

Table 8: The feature cosine of each bus and judgment results in different SNR.

(a) SNR=50db

F_t R_f F_L O_m	P	[B_1, B_2, B_3, B_4, B_5]	Each P result	Final result
LG(a)	a	[0.907, -0.945, -0.909, -0.527, -0.352]	healthy	
5Ω	b	[0.999, 0.999, 0.999, -0.995, -0.993]	B_1-B_2	B_1-B_2
B_1-B_2 islanded	c	[0.999, 0.999, 0.999, -0.996, -0.995]	healthy	
LLG(ab)	a	[0.535, 0.920, -0.064, -0.899, 0.073]	B_2-B_3	
1Ω	b	[0.754, 0.939, 0.039, -0.938, -0.726]	healthy	B_2-B_3
B_2-B_3 islanded	c	[0.995, 1.000, -1.000, -0.964, -0.940]	B_2-B_3	
LLLG	a	[-0.641, 0.450, 0.275, -0.283, 0.377]	B_4-B_5	
5Ω	b	[-0.967, 0.913, 0.768, -1.000, 0.964]	B_4-B_5	B_4-B_5
B_4-B_5 Grid	c	[0.699, 0.677, 0.647, -0.858, 1.000]	B_4-B_5	

(b) SNR=5db

F_t R_f F_L O_m	P	[B_1, B_2, B_3, B_4, B_5]	Each P result	Final result
LG(a)	a	[0.907, -0.945, -0.909, -0.527, -0.352]	healthy	
5Ω	b	[0.999, 0.999, 0.999, -0.995, -0.993]	B_1-B_2	B_1-B_2
B_1-B_2 islanded	c	[0.999, 0.999, 0.999, -0.996, -0.996]	healthy	
LLG(ab)	a	[0.535, 0.920, -0.064, -0.899, 0.073]	B_2-B_3	
1Ω	b	[0.754, 0.939, -0.100, -0.958, -0.726]	healthy	B_2-B_3
B_2-B_3 islanded	c	[0.995, 1.000, 1.000, -0.974, -0.940]	B_2-B_3	
LLLG	a	[-0.643, -0.450, -0.275, 0.283, -0.377]	B_4-B_5	
5Ω	b	[-0.970, -0.913, -0.768, 1.000, -0.964]	B_4-B_5	B_4-B_5
B_4-B_5 Grid	c	[-0.699, -0.677, -0.647, 0.858, -1.000]	B_4-B_5	

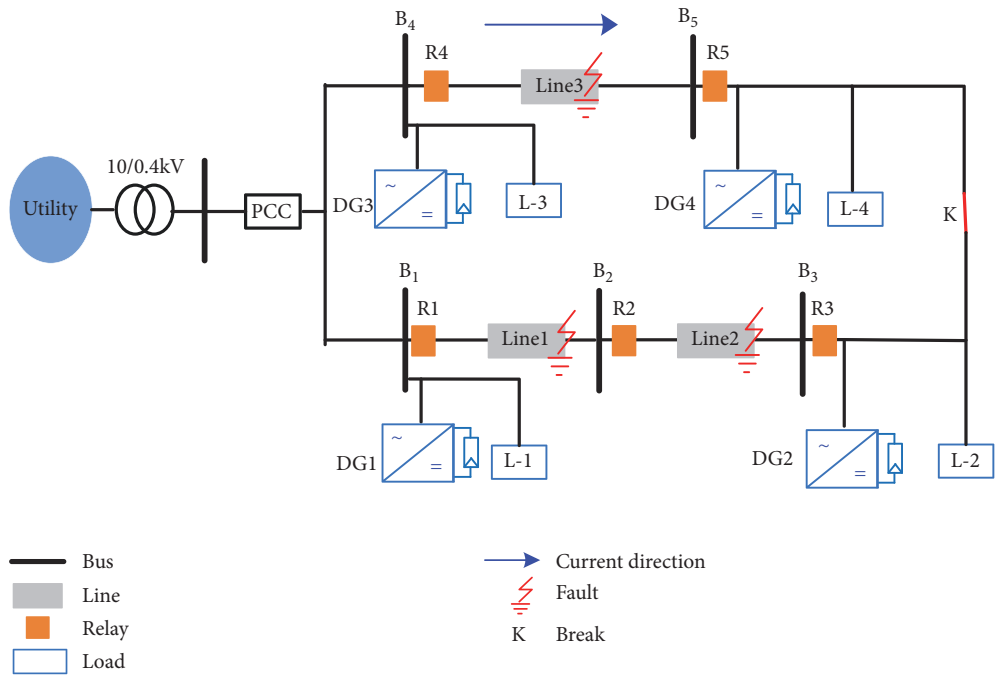

Figure 10: The looped microgrid.

Table 9: The feature cosine of each bus and judgment results for the looped microgrid.

F_t R_f F_L O_m	P	[B_1, B_2, B_3, B_4,B_5]	Each P result	Final result
LG(a)	a	[0.965, -0.973, -0.949, -0.790, -0.741]	B_1- B_2	
0.1Ω	b	[-1.102, -1.103, -1.103, -1.098, -1.100]	healthy	B_1- B_2
B_1-B_2 islanded	c	[-1.043, -1.044, -1.044, -1.040, -1.041]	healthy	
LLG(ab)	a	[0.932, 0.978, -0.929, 0.958, 0.980]	B_2- B_3	
0.1Ω	b	[0.535, 0.763, -0.500, 0.657, 0.788]	B_2- B_3	B_2- B_3
B_2-B_3 islanded	c	[0.997, 0.998, 0.998, 0.997, 0.998]	healthy	
LLLG	a	[-0.906, -0.896, -0.887, 0.691, -0.673]	B_4- B_5	
0.1Ω	b	[-0.654, -0.612, -0.583, 0.561, -0.480]	B_4- B_5	B_4- B_5
B_4-B_5 islanded	c	[-1.032, -1.032, -1.031, 0.918, -0.932]	B_4- B_5	
LG(b)	a	[0.534, -0.953, -0.912, 0.386, 0.939]	B_1- B_2	
1Ω	b	[1.275, 0.767, 0.933, 1.273, 0.933]	healthy	B_1- B_2
B_1-B_2 Grid	c	[0.647, 0.764, 0.928, 0.645, 0.928]	healthy	
LLG(ac)	a	[0.393, 0.935, -0.788, 0.673, 0.938]	B_2- B_3	
1Ω	b	[-0.357, 0.880, 1.007, -0.357, 1.006]	healthy	B_2- B_3
Grid B_2-B_3	c	[0.357, 0.953, -0.856, 0.724, 0.937]	B_2- B_3	
LLLG	a	[0.551, 0.746, 0.819, 0.531, -0.831]	B_4- B_5	
1Ω	b	[0.442, 0.588, 0.662, 0.292, -0.503]	B_4- B_5	B_4- B_5
Grid B_4-B_5	c	[0.907, 1.039, 1.067, 1.006, -1.051]	B_4- B_5	

Table 10: The feature cosine of each bus and judgment results for the sample microgrid.

F_t R_f F_L O_m	P	[B_1, B_2, B_3, B_4,B_5]	Each P result	Final result
LG(a)	a	[0.762, -0.981, -0.980, -0.976, -0.973]	B_1- B_2	B_1- B_2
0.3Ω	b	[-0.988, -0.987, -0.987, -0.981, -0.973]	healthy	
B_1-B_2 islanded	c	[-0.987, -0.987, -0.987, -0.981, -0.971]	healthy	
LLG(ab)	a	[1.087, 1.006, -0.973, -0.990, -0.988]	B_2- B_3	B_2- B_3
0.3Ω	b	[0.310, 0.689, -0.969, -0.950, -0.944]	B_2- B_3	
B_2-B_3 islanded	c	[-0.984, -0.984, -0.983, -0.976, -0.974]	healthy	
LLL	a	[-0.978, -0.977, -0.977, 0.427, -0.965]	B_4- B_5	B_4- B_5
/	b	[-0.973, -0.972, -0.971, 0.291, -0.956]	B_4- B_5	
B_4-B_5 islanded	c	[-0.971, -0.970, -0.970, 0.420, -0.956]	B_4- B_5	
LG(b)	a	[-0.990, -0.990, -0.989, -0.981, -0.978]	healthy	B_1- B_2
3Ω	b	[0.071, -1.027, -1.027, -1.152, -1.159]	B_1- B_2	
B_1-B_2 Grid	c	[-0.989, -0.989, -0.989, -0.981, -0.978]	healthy	
LLG(ac)	a	[0.435, 0.966, -0.979, -0.949, -0.946]	B_2- B_3	B_2- B_3
3Ω	b	[-0.976, -0.976, -0.976, -0.965, -0.961]	healthy	
Grid B_2-B_3	c	[0.563, 0.967, -0.979, -0.952, -0.945]	B_2- B_3	
LLLG	a	[-0.977, -0.976, -0.976, 0.283, -0.965]	B_4- B_5	B_4- B_5
3Ω	b	[-0.965, -0.964, -0.963, 0.246, -0.956]	B_4- B_5	
Grid B_4-B_5	c	[-0.962, -0.962, -0.961, 0.447, -0.956]	B_4- B_5	

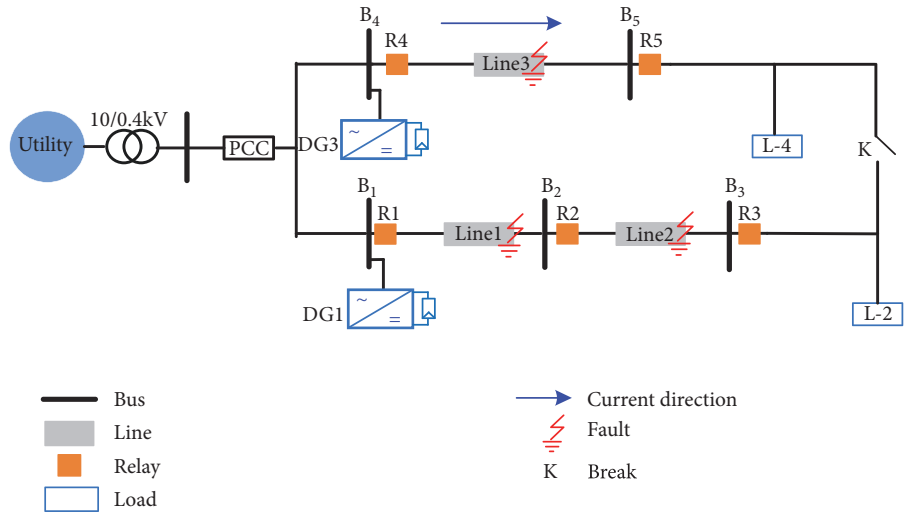

Figure 11: Sample microgrid whose nodes are with only loads.

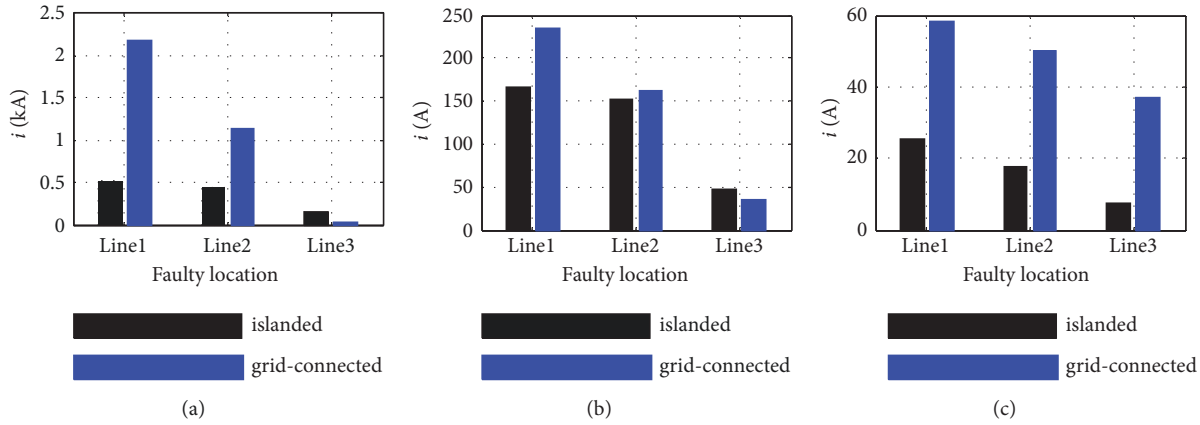

FIGURE 12: Fault current peak value of B_1 in different R_f. (a) 0.01Ω; (b) 1Ω; (c) 10Ω.

and current to calculate the differential direction; this method is found to work effectively under various case studies as discussed in this paper including different grounding resistances and faulty types. The advantage of the proposed method is that it is not needed to change the threshold to detect the faulty section location when the microgrid operation mode is changed and has unbalanced loads.

Data Availability

The data used to support the findings of this study are available from the corresponding author upon request.

Conflicts of Interest

The authors declare that there are no conflicts of interest regarding the publication of this article.

Acknowledgments

This work is supported by University-Level Scientific Research Project (ZEPCKY2019-01) of Zhengzhou Electric Power College, China.

References

[1] H. Xiao, A. Luo, Z. Shuai, G. Jin, and Y. Huang, "An improved control method for multiple bidirectional power converters in hybrid AC/DC microgrid," *IEEE Transactions on Smart Grid*, vol. 7, no. 1, pp. 340–347, 2016.

[2] X. Wang, J. Gao, X. Wei et al., "High impedance fault detection method based on variational mode decomposition and Teager-Kaiser energy operators for distribution network," *IEEE Transactions on Smart Grid, Early Access*, p. 1, 2019.

[3] X. Wang, J. Gao, M. Chen, X. Wei, Y. Wei, and Z. Zeng, "Faulty line detection method based on optimized bistable system for distribution network," *IEEE Transactions on Industrial Informatics*, vol. 14, no. 4, pp. 1370–1381, 2018.

[4] A. Hooshyar and R. Iravani, "Microgrid protection," *Proceedings of the IEEE*, vol. 105, no. 7, pp. 1332–1353, 2017.

[5] X. Liu, M. Shahidehpour, Z. Li, X. Liu, Y. Cao, and W. Tian, "Protection scheme for loop-based microgrids," *IEEE Transactions on Smart Grid*, vol. 8, no. 3, pp. 1340–1349, 2017.

[6] S. Teimourzadeh, F. Aminifar, M. Davarpanah, and M. Shahidehpour, "Adaptive protection for preserving microgrid security," *IEEE Transactions on Smart Grid*, vol. 10, no. 1, pp. 592–600, 2019.

[7] Z. Chen, X. Pei, M. Yang, L. Peng, and P. Shi, "A novel protection scheme for inverter-interfaced microgrid (IIM) operated in islanded mode," *IEEE Transactions on Power Electronics*, vol. 33, no. 9, pp. 7684–7697, 2018.

[8] H. J. Laaksonen, "Protection principles for future microgrids," *IEEE Transactions on Power Electronics*, vol. 25, no. 12, pp. 2910–2918, 2010.

[9] H. Muda and P. Jena, "Superimposed adaptive sequence current based microgrid protection: a new technique," *IEEE Transactions on Power Delivery*, vol. 32, no. 2, pp. 757–767, 2017.

[10] S. Mirsaeidi, D. M. Said, M. W. Mustafa, and M. H. Habibuddin, "A protection strategy for micro-grids based on positive-sequence component," *IET Renewable Power Generation*, vol. 9, no. 6, pp. 600–609, 2015.

[11] J. Duan, K. Zhang, and L. Cheng, "A novel method of fault location for single-phase microgrids," *IEEE Transactions on Smart Grid*, vol. 7, no. 2, pp. 915–925, 2016.

[12] S. A. Saleh, R. Ahshan, M. S. Abu-Khaizaran, B. Alsayid, and M. A. Rahman, "Implementing and testing d-q WPT-based digital protection for microgrid systems," *IEEE Transactions on Industry Applications*, vol. 50, no. 3, pp. 2173–2185, 2014.

[13] A. Gururani, S. R. Mohanty, and J. C. Mohanta, "Microgrid protection using Hilbert-Huang transform based-differential scheme," *IET Generation, Transmission & Distribution*, vol. 10, no. 15, pp. 3707–3716, 2016.

[14] S. Kar and S. R. Samantaray, "Time-frequency transform-based differential scheme for microgrid protection," *IET Generation, Transmission & Distribution*, vol. 8, no. 2, pp. 310–320, 2014.

[15] E. Casagrande, W. L. Woon, H. H. Zeineldin, and N. H. Kan'an, "Data mining approach to fault detection for isolated inverter-based microgrids," *IET Generation, Transmission & Distribution*, vol. 7, no. 7, pp. 745–754, 2013.

[16] E. Casagrande, W. L. Woon, H. H. Zeineldin, and D. Svetinovic, "A differential sequence component protection scheme for microgrids with inverter-based distributed generators," *IEEE Transactions on Smart Grid*, vol. 5, no. 1, pp. 29–37, 2014.

[17] D. P. Mishra, S. R. Samantaray, and G. Joos, "A combined wavelet and data-mining based intelligent protection scheme for microgrid," *IEEE Transactions on Smart Grid*, vol. 7, no. 5, pp. 2295–2304, 2016.

[18] S. Kar, S. R. Samantaray, and M. D. Zadeh, "Data-mining model based intelligent differential microgrid protection scheme," *IEEE Systems Journal*, vol. 11, no. 2, pp. 1161–1169, 2017.

[19] A. De Souza Gomes, M. A. Costa, T. G. A. Defaria, and W. M. Caminhas, "Detection and classification of faults in power transmission lines using functional analysis and computational intelligence," *IEEE Transactions on Power Delivery*, vol. 28, no. 3, pp. 1402–1413, 2013.

[20] C. Ma and L. Jiang, "Some research on Levenberg-Marquardt method for the nonlinear equations," *Applied Mathematics and Computation*, vol. 184, no. 2, pp. 1032–1040, 2007.

[21] P. Piagi and R. H. Lasseter, "Autonomous control of microgrids," in *Proceedings of the 2006 IEEE Power Engineering Society General Meeting, PES*, Canada, June 2006.

[22] K. Yu, Q. Ai, S. Wang, J. Ni, and T. Lv, "Analysis and optimization of droop controller for microgrid system based on small-signal dynamic model," *IEEE Transactions on Smart Grid*, vol. 7, no. 2, pp. 695–705, 2016.

[23] M. Yazdanian and A. Mehrizi-Sani, "Washout filter-based power sharing," *IEEE Transactions on Smart Grid*, vol. 7, no. 2, pp. 967-968, 2016.

[24] K. O. Oureilidis and C. S. Demoulias, "A fault clearing method in converter-dominated microgrids with conventional protection means," *IEEE Transactions on Power Electronics*, vol. 31, no. 6, pp. 4628–4640, 2016.

[25] B. Dag, A. R. Boynuegri, Y. Ates, A. Karakas, A. Nadar, and M. Uzunoglu, "Static modeling of microgrids for load flow and fault analysis," *IEEE Transactions on Power Systems*, vol. 32, no. 3, pp. 1990–2000, 2017.

[26] B. Jiang, L. Mu, W. Guo, and W. Zhuang, "Microgrid protection based on change of measured bus admittance," *Power System Technology*, vol. 39, no. 6, pp. 1751–1758, 2015.

[27] H. Zhang, T. R. Blackburn, B. T. Phung, and D. Sen, "A novel wavelet transform technique for on-line partial discharge measurements part 1: WT de-noising algorithm," *IEEE Transactions on Dielectrics and Electrical Insulation*, vol. 14, no. 1, pp. 3–14, 2007.